Dynamic State Estimation for Power Systems with Uncertain Inputs

Heqing Huang, *Graduate Student Member, IEEE*, Yuzhang Lin, *Member, IEEE*

***Abstract*—Traditional Dynamic State Estimation (DSE) techniques focus on the filtering of noise and gross errors in output variables, which are commonly assumed to come from measurements. In power systems, however, input variables may have substantial uncertainty as well, as many of them are also measured or telecommunicated signals. This paper discusses the impact of uncertainty in different types of inputs and proposes an Adaptive Iterated Cubature Kalman Filter with Uncertain Input (AICKF-UcI) approach to systematically handling this problem. In the prediction stage, the method utilizes the Cubature transform to address system nonlinearity. Then, it converts the correction stage into a problem akin to Weighted Least Squares (WLS) regression, enabling iterative joint estimation of the state and uncertain input. Additionally, this method incorporates an adaptive algorithm for real-time estimation of noise distribution. Furthermore, the method is devised to have the unique capability of detecting and suppressing gross errors in input variables, and differentiating them from those in output variables. The advantages and versatility of the proposed method are validated through DSE on a Permanent Magnet Synchronous Generator (PMSG) based wind turbine in a distribution system and a synchronous generator (SG) in a transmission system.**

***Index Terms*—adaptive estimation, cubature Kalman filter, dynamic state estimation, inverter-based resources, power grid monitoring, situational awareness, uncertain input**

I. Introduction

THE modern power system is faced with numerous operational challenges as the penetration of renewable energy increases. The widespread deployment of Inverter-Based Resources (IBRs) complicates the dynamic characteristics of the power system with a broader time scale, less inertia, a more distributed structure, and more diverse control strategies. To address these challenges, system operators require enhanced monitoring and situational awareness capabilities to dispatch, stabilize, and protect the grid. Leveraging high-resolution measurement data emerging in power systems, such as PMU (Phasor Measurement Unit) and merged units [1], Dynamic State Estimation (DSE) has become a promising technique that may potentially provide these functionalities to system operators. Popular estimation methods for dynamic systems, such as Extended Kalman Filtering (EKF) [2], Unscented Kalman Filtering (UKF) [3], Cubature Kalman Filtering (CKF) [4], Ensemble Kalman Filtering (EnKF) [5], and Particle Filtering (PF) [6], have been applied to the DSE of power systems, as have been thoroughly reviewed in [7].

Conventional estimation methods [2]–[6] mentioned above are all based on several common assumptions about the dynamic system, such as known model structures, parameters, inputs, and measurements of system outputs, and the process noise and measurement noise have known (typically Gaussian) distributions. In practice, however, assuming that all the aforementioned information is completely known may not always be realistic. To handle the issue of estimator instability caused by unknown non-Gaussian noise and gross errors, various robust estimators have been proposed. Ref. [8] combines the generalized correntropy (GC) loss with Adaptive CKF (ACKF), forming AGCLCKF, to address this issue, with results reported on the New England 68-bus test system. Ref. [9] adopts a similar approach to Ref. [8], integrating the generalized maximum correntropy criterion with EnKF to form GMCC-EnKF, which effectively implements DSE for Doubly-Fed Induction Generator (DFIG) wind turbines under non-Gaussian noise. Ref. [10] combines the IEKF with the generalized maximum likelihood approach to form a GM-IEKF technique. The robust KF framework can also be utilized to address the issue of inaccurate model parameters [11], and it is shown that joint estimation of parameters and states is feasible [12]. To mitigate the impact of non-Gaussian noise and randomly occurring denial-of-service (DoS) attacks, Ref. [13] proposes an resilient DSE method by combining the Cauchy kernel maximum correntropy (CKMC) optimal criterion with the CKF (CKMC-CKF) and verifies the effectiveness of this method in the IEEE 39-bus system.

Apart from unknown noise distributions and inaccurate model parameters, another practical challenge is the difficulty in obtaining complete and accurate input information. To cope with the challenge of unknown inputs, various novel DSE methods have emerged. One of the most popular family of approaches is the variation of KF methods with Unknown Input (UI), referred to as xKF-UI in this paper. Ref. [14] employs the EKF-UI method, where the torque obtained from the previous step is used as an input during the prediction step. The unknown input and state of the SG are jointly updated in the correction step. Ref. [15] uses the CKF-UI to estimate the unknown inputs of SGs. This method involves an initial biased CKF step, followed by the correction of the unknown input using the output information. Subsequently, an unbiased CKF step is carried out using the corrected unknown input. Ref. [16] employs CKF-UI to perform joint estimation of unknown wind speed and states for DFIG wind turbines. A notable difference from the conventional CKF-UI is that after the biased estimation, the relation between the unknown input and measurements is directly obtained through power series. Ref. [17] builds upon the CKF-UI and introduces an adaptive interpolation process to enhance stability. Ref. [18] extends the UKF-UI and includes the estimation of process noise distribution. In addition to the xKF-UI framework, there are other methods to address UIs in DSE. For example, Ref.

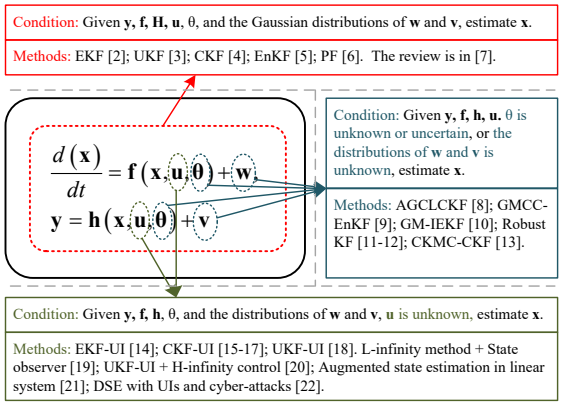

Fig. 1. The main areas and distinctions in DSE research within power systems.

[19] utilizes the L-infinity method to design a state observer, assuming the system possesses local Lipschitz stability and guarantees the state estimation error norm relative to the worst case disturbance. Ref. [20] combines UKF-UI with H-Infinity control principles to achieve satisfactory estimation results with non-Gaussian noise. For distribution networks, Ref. [21] constructs a linear system and performs augmented state estimation in the presence of UIs. Ref. [22] proposes a DSE method for SGs in the presence of both cyber-attacks and UIs with a linear system model.

Overall, current DSE research in power systems primarily focuses on three areas, which addresses different problems associated with a dynamic power system model as shown in Fig. 1. The first area addresses the classical DSE problem, which assumes complete knowledge of the system information and focuses on estimating dynamic state variables. The second area addresses the DSE problem when the noise distribution is unknown or when there is uncertainty in the parameters. The final area addresses the problem where some input parameters are unknown, specifically in the presence of UIs. Despite the reported effectiveness of the aforementioned DSE methods for systems with UIs, a vast majority of the existing DSE methods still have "bipolar" assumptions about input variables in power systems: they are either assumed to be precisely known, or assumed to be completely unknown (as indicated by the names of the methods, with the term "unknown input"). In many practical situations in power systems, however, the inputs are not precisely known nor completely unknown, meaning that some information is provided about the inputs, but with uncertainty (both noise and gross errors). This happens when the inputs also come from measurement devices just as the outputs, or from remote agents via communication subject to corruptions. For instance, in the DSE models of SGs, the terminal voltage phasor is treated as an input, and the terminal current phasor is treated as an output [14], [23]. While it is recognized in conventional methods that the output (current phasor) comes from measurement devices (PMUs in this case) with imperfection, it is commonly ignored that the input (terminal voltage phasor) is also obtained from PMU measurements and is subject to noise and gross errors as well. In addition, it is often assumed that the excitation current is a completely unknown input, while it is actually possible to transmit its measurements, although it may carry noise or gross errors. Similar situations also exist in the DSE of IBRs. Unlike the assumptions of existing works that wind speeds are completely unknown inputs [16], [17], wind turbines commonly have wind speed sensors, while their low sampling rates and accuracy levels create significant uncertainty in the measurements. All the examples described above involve the condition of ***Uncertain Input (UcI)*** (as opposed to *Unknown Input (UI)*), for which limited research has been conducted. One approach is to incorporate these uncertainties into the process noise [23], [24]. However, when the noise of input variables are propagated through the state transition equations, they will yield correlated uncertainty between different states, which cannot be accurately characterized by the independent process noise model. Furthermore, these methods lack the capability of detecting and suppressing the impact of gross errors (leading to anomalies or bad data) in the inputs, which do not follow probability distributions assumed by the estimator.

In view of the aforementioned challenges, we propose an innovative Adaptive Iterated CKF with Uncertain Inputs (AICKF-UcI) to harvest uncertain information about inputs, providing an effective DSE solution to many practical applications such as the monitoring of SGs and IBRs. The main contributions are summarized as follows.

1) A universal AICKF-UcI framework is proposed for dynamic systems with various types of input structures. By reformulating the state transition equations and defining three different types of inputs, it enables the joint estimation of state variables and all types of inputs appearing in both the state transitions and/or output equations.

2) By devising an extended noise estimation algorithm, the statistics (i.e., variances) of noises in input variables can be estimated, and the optimal filtering performances can be achieved online. The propagation of input noise through nonlinear state and output equations are also accurately modeled.

3) The integration of the Largest Normalized Residual (LNR) method into the AICKF-UcI framework allows explicit and accurate detection and correction of bad data in input variables, which is commonly mistakenly blamed as bad data in output variables in conventional methods due to their inability to inspect input variables.

The effectiveness of the proposed method is validated on a virtual system test case with all types of input structures, followed by practical power system test cases with both SGs and IBRs, and both transmission and distribution systems.

II. Adaptive Iterated CKF with Uncertain Inputs

A. Problem Formulation

A continuous-time dynamic system with inputs is commonly described by state transition equations and output equations written as follows:

$$\begin{cases} \frac{d(\mathbf{x})}{dt} = \mathbf{f}_c(\mathbf{x}, \mathbf{u}, \theta) + \mathbf{w}, \\ \bar{\mathbf{y}} = \mathbf{h}_c(\mathbf{x}, \mathbf{u}, \theta) + \mathbf{v}, \end{cases} \tag{1}$$

where $\mathbf{f}_c$ and $\mathbf{h}_c$ respectively denote the state transition function and output function of the continuous system; $\mathbf{x} \in \mathbb{R}^{n_x \times 1}$ is the state variables; $\mathbf{u} \in \mathbb{R}^{n_u \times 1}$ is the external inputs; $\bar{\mathbf{y}} \in \mathbb{R}^{n_y \times 1}$ is the measurements of output; θ is the parameters

of the system, and $\mathbf{w}$ and $\mathbf{v}$ represent process noise and measurement noise, respectively.

Discretizing (1) yields:

$$\begin{cases} \mathbf{x}_{k+1} = \mathbf{f}\left(\mathbf{x}_k, \mathbf{u}_k, \theta\right) + \mathbf{w}_k, \\ \bar{\mathbf{y}}_{k+1} = \mathbf{h}\left(\mathbf{x}_{k+1}, \mathbf{u}_{k+1}, \theta\right) + \mathbf{v}_{k+1}, \end{cases} \tag{2}$$

where k represents the time step, $\mathbf{f}$ and $\mathbf{h}$ respectively denote the state transition function and output function of the discretized system.

The currently prevalent DSE methods involving UIs extends system formulation (2) as follows:

$$\begin{cases} \mathbf{x}_{k+1} = \mathbf{f}\left(\mathbf{x}_k, \mathbf{u}_k, \theta\right) + \mathbf{G}\mathbf{d}_k + \mathbf{w}_k, \\ \bar{\mathbf{y}}_{k+1} = \mathbf{h}\left(\mathbf{x}_{k+1}, \mathbf{u}_{k+1}, \theta\right) + \mathbf{v}_{k+1}, \end{cases} \tag{3}$$

where $\mathbf{d}$ represents UIs, and $\mathbf{u}$ represents known and deterministic inputs. This representation differentiates UIs from known inputs, separating the influences of UIs on the state transition equations from those of the other inputs. It facilitates the joint estimation of state variables and UIs.

However, as mentioned in the Section I, the xKF-UI framework with Eq. (3) assumes inputs to be either exactly known (error-free) or completely unknown, which does not reflect many scenarios in the real world. Moreover, there are two more limitations that were not mentioned in Section I. 1) The influences of the UIs on the state transition are linearized, which may introduce large errors in systems with strong nonlinearity. 2) In general, UIs can appear in different structures in the equations, i.e., only in state transition equations, only in output equations, or in both set of equations. The representation used in existing works, Eq. (3), can only handle the first structure, not the second and third ones.

To overcome the limitations of (3) widely used in existing works, this paper proposes a generic formulation as follows:

$$\begin{cases} \mathbf{x}_{k+1} = \mathbf{f}\left(\mathbf{x}_k, \mathbf{u}_k^a, \mathbf{u}_k^f, \theta\right) + \mathbf{w}_k, \\ \bar{\mathbf{y}}_{k+1} = \mathbf{h}\left(\mathbf{x}_{k+1}, \mathbf{u}_{k+1}^a, \mathbf{u}_{k+1}^h, \theta\right) + \mathbf{v}_{k+1}, \\ \bar{\mathbf{u}}_{k+1}^{\phi} = \mathbf{u}_{k+1}^{\phi} + \mathbf{c}_{k+1}^{\phi}, \phi \in \{a, h\} \\ \bar{\mathbf{u}}_k^f = \mathbf{u}_k^f + \mathbf{c}_k^f. \end{cases} \tag{4}$$

where $\mathbf{u}^a \in \mathbb{R}^{n_a \times 1}$ represents inputs that influence both the output equations and the state transition equations simultaneously; $\mathbf{u}^f \in \mathbb{R}^{n_f \times 1}$ represents inputs that only influence the state transition equations; and $\mathbf{u}^h \in \mathbb{R}^{n_h \times 1}$ represents inputs that only influence the output equations. Meanwhile, as mentioned earlier, the true values of the inputs cannot be obtained; rather, the measured values of the inputs $\bar{\mathbf{u}}_{k+1}^{\phi}$ are available with noise $\mathbf{c}_{k+1}^{\phi}$ where $\phi \in \{a, h\}$; similarly, for the control input $\mathbf{u}_k^f$ applied to the state transition equation at the time step k, we can only obtain its noisy measurement $\bar{\mathbf{u}}_{\mathbf{k}}^{\mathbf{f}}$. It should be noted that a practical system may not always include all three types of inputs. However, the proposed formulation (4) provides a comprehensive representation of systems with UcIs, allowing the proposed DSE algorithm to address systems with all types of input structures. By employing Eq. (4) to describe the UcI problem, we can qualitatively understand the relationship between different inputs and outputs. For instance, we can estimate $\mathbf{u}_k^a$ and $\mathbf{u}_k^h$ solely using the outputs, while the estimation of $\mathbf{u}_{k-1}^f$ is also influenced by the state transition equation; the estimation of $\mathbf{u}_k^a$ will affect the state transition equation in the next time step, thus the impact of the previous step's estimation accuracy of $\mathbf{u}_k^a$ on DSE needs to be considered. For detailed analysis, please refer to Section II-C. It is also evident from Eq. (4) that, unlike traditional state variables, the transition rule of inputs is not known, and therefore, only the output equations are available for them. This difference prevents the traditional KF framework from being directly applied to UcI problems, necessitating the development of a new framework (AICKF-UcI) to achieve joint estimation of state variables and input variables.

B. The Proposed AICKF-UcI Algorithm

Following the Section II-A, the proposed AICKF-UcI method explicitly recognizes the uncertainty of input variables and extends the traditional KF framework to filter the uncertainty. It equivalently transforms the correction step of the KF problem with UcIs into a weighted least squares (WLS) regression problem, while still employing the Cubature transform to mitigate the impact of system nonlinearity in state transition equation. Mechanisms for handling the estimation of unknown noise variances and the detection and correction of gross errors (leading to bad data) are also integrated for both input and output variables. The specific steps are as follows.

1) Initialization. Set time step $k = 0$, and initialize the posterior estimate of the state variables $\widehat{\mathbf{x}}_{k(+)}$ and the covariance matrix $\widehat{\mathbf{P}}_{k(+)}$; initialize the posterior estimate of $\mathbf{u}_{k(+)}^a$ and the covariance matrix $\mathbf{C}_{k(+)}^a$.

2) Time increment. Set $k \leftarrow k + 1$.

3) Prediction. According to Eq. (4), to predict the state variables at time step k, it is necessary to have the posterior estimate of the state variables at time step $k-1$, $\widehat{\mathbf{x}}_{k-1(+)}$, the posterior estimate of $\mathbf{u}^a$, $\mathbf{u}_{k-1(+)}^a$, and the value of $\mathbf{u}_{k-1(+)}^f$. The first two can be obtained from the previous time step, while the last item needs to be iteratively updated. The equations for the prediction step are written as follows:

$$\widehat{\mathbf{x}}_{k(-)} = \mathbf{f}\left(\begin{bmatrix} \widehat{\mathbf{x}}_{k-1(+)} \\ \widehat{\mathbf{u}}_{k-1(+)}^a \end{bmatrix}, \mathbf{u}_{k-1}^f\right). \tag{5}$$

For Eq. (5), $\widehat{\mathbf{x}}_{k-1(+)}$ and $\widehat{\mathbf{u}}_{k-1(+)}^a$ are known, and their covariance matrices can be obtained from the previous DSE process, denoted as $\widehat{\mathbf{P}}_{k-1(+)}^{xu^a}$. However, $\mathbf{u}_{k-1}^f$ needs to be updated through the correction step. The latest $\mathbf{u}_{k-1}^f$ can be used for computation in each iteration. As the state transition equations are nonlinear, a first-order Taylor expansion, as done in the EKF approach, can introduce significant errors. Therefore, we use the Cubature transform method to predict the state variables and their covariance matrix at time step k. The Cubature points are computed as:

$$\chi_{i,k-1|k-1} = \left(\widehat{\mathbf{P}}_{k-1(+)}^{xu^a}\right)^{\frac{1}{2}} \zeta_i + \begin{bmatrix} \widehat{\mathbf{x}}_{k-1(+)} \\ \widehat{\mathbf{u}}_{k-1(+)}^a \end{bmatrix}, \tag{6}$$

where ζ_i represents the i-th column of matrix $\sqrt{n_x + n_a}\left[I_{n_x+n_a}, -I_{n_x+n_a}\right]$ ($I_{n_x+n_a}$ represents the $n_x + n_a$

dimensional identity matrix). Propagate them through the state equations:

$$\chi_{i,k|k-1} = \mathbf{f}\left(\chi_{i,k-1|k-1}, \mathbf{u}_{k-1}^{f}\right). \tag{7}$$

Then, we can obtain the predicted values of the state variables along with their covariance matrix:

$$\widehat{\mathbf{x}}_{k(-)} = \frac{1}{2\left(n_x+n_a\right)} \sum_{i=1}^{n_x+n_a} \chi_{i,k|k-1}, \tag{8}$$

$$\widehat{\mathbf{P}}_{k(-)} = \frac{\chi_{k|k-1}\chi_{k|k-1}^{T}}{2\left(n_x+n_a\right)} - \widehat{\mathbf{x}}_{k(-)}\widehat{\mathbf{x}}_{k(-)}^{T} + \mathbf{Q}_{k-1}. \tag{9}$$

4) Correction in the form of WLS regression. Ref. [25] utilizes the Matrix Inversion Lemma (MIL) and Gain Expression (GE) Identity to demonstrate that in the EKF, the correction step can be equivalently represented as a WLS problem, and the traditional EKF obtains the solution to this problem. Leveraging this elegant conclusion, here the correction step is also transformed into a WLS problem:

$$\begin{aligned}\widehat{\mathbf{x}}_{k(+)} = \arg\min_{\mathbf{x}_k} \Big\{ &\left(\widehat{\mathbf{x}}_{k(-)} - \mathbf{x}_k\right)^{T} \widehat{\mathbf{P}}_{k(-)}^{-1} \left(\widehat{\mathbf{x}}_{k(-)} - \mathbf{x}_k\right) \\ &+ \left(\bar{\mathbf{y}}_k - \mathbf{h}\left(\mathbf{x}_k, \bar{\mathbf{u}}_k\right)\right)^{T} \mathbf{R}_k^{-1} \left(\bar{\mathbf{y}}_k - \mathbf{h}\left(\mathbf{x}_k, \bar{\mathbf{u}}_k\right)\right) \Big\}.\end{aligned} \tag{10}$$

For systems with UcIs, however, the three different types of inputs also need to be estimated. Meanwhile, we have noisy measurements for each input. Therefore, the above-mentioned WLS can be augmented as follows:

$$\begin{aligned}\arg\min_{\mathbf{x}_k, \mathbf{u}_k^a, \mathbf{u}_{k-1}^f, \mathbf{u}_k^h} \Big\{ &\left(\widehat{\mathbf{x}}_{k(-)} - \mathbf{x}_k\right)^{T} \widehat{\mathbf{P}}_{k(-)}^{-1} \left(\widehat{\mathbf{x}}_{k(-)} - \mathbf{x}_k\right) \\ &+ \left(\bar{\mathbf{u}}_k^a - \mathbf{u}_k^a\right)^{T} \left(\mathbf{C}_k^a\right)^{-1} \left(\bar{\mathbf{u}}_k^a - \mathbf{u}_k^a\right) \\ &+ \left(\bar{\mathbf{u}}_{k-1}^f - \mathbf{u}_{k-1}^f\right)^{T} \left(\mathbf{C}_{k-1}^f\right)^{-1} \left(\bar{\mathbf{u}}_{k-1}^f - \mathbf{u}_{k-1}^f\right) \\ &+ \left(\bar{\mathbf{u}}_k^h - \mathbf{u}_k^h\right)^{T} \left(\mathbf{C}_k^h\right)^{-1} \left(\bar{\mathbf{u}}_k^h - \mathbf{u}_k^h\right) \\ &+ \left(\bar{\mathbf{y}}_k - \mathbf{h}\left(\mathbf{x}_k, \mathbf{u}_k^a, \mathbf{u}_k^h\right)\right)^{T} \mathbf{R}_k^{-1} \left(\bar{\mathbf{y}}_k - \mathbf{h}\left(\mathbf{x}_k, \mathbf{u}_k^a, \mathbf{u}_k^h\right)\right) \Big\},\end{aligned} \tag{11}$$

where $\bar{\mathbf{u}}_k^a$, $\bar{\mathbf{u}}_{k-1}^f$, and $\bar{\mathbf{u}}_k^h$ respectively represent the measured values of the three types of inputs, which may carry noise and even gross errors (to be handled in a subsequent step); $\mathbf{C}_k^a$, $\mathbf{C}_{k-1}^f$, and $\mathbf{C}_k^h$ are the covariance matrices of these measured values, respectively. We can concatenate all the unknown variables as an augmented state vector, $\tilde{\mathbf{x}}_k = \left[\mathbf{u}_{k-1}^f, \mathbf{x}_k, \mathbf{u}_k^a, \mathbf{u}_k^h\right]^{T}$. Then the augmented output equations can be expressed as follows:

$$\tilde{\mathbf{h}}\left(\tilde{\mathbf{x}}_k\right) = \begin{bmatrix} \mathbf{u}_{k-1}^f \\ \mathbf{x}_k - \widehat{\mathbf{x}}_{k(-)} \\ \mathbf{u}_k^a \\ \mathbf{u}_k^h \\ \mathbf{h}\left(\mathbf{x}_k, \mathbf{u}_k^a, \mathbf{u}_k^h\right) \end{bmatrix}. \tag{12}$$

Similarly, we construct an augmented measurement vector $\tilde{\mathbf{y}}_k = \left[\bar{\mathbf{u}}_{k-1}^f, \mathbf{0}, \bar{\mathbf{u}}_k^a, \bar{\mathbf{u}}_k^h, \bar{\mathbf{y}}_k\right]^{T}$. Then problem (11) can be rewritten as follows:

$$\begin{aligned}\tilde{\mathbf{x}}_k &= \arg\min_{\tilde{\mathbf{x}}_k} \left\{ \left(\tilde{\mathbf{y}}_k - \tilde{\mathbf{h}}\left(\tilde{\mathbf{x}}_k\right)\right)^{T} \tilde{\mathbf{R}}_k^{-1} \left(\tilde{\mathbf{y}}_k - \tilde{\mathbf{h}}\left(\tilde{\mathbf{x}}_k\right)\right) \right\}, \\ \tilde{\mathbf{R}}_k &= diag\left(\mathbf{C}_{k-1}^f, \widehat{\mathbf{P}}_{k(-)}, \mathbf{C}_k^a, \mathbf{C}_k^h, \mathbf{R}_k\right).\end{aligned} \tag{13}$$

Eq. (13) formally adheres to the structure expected of a WLS problem. However, according to Eq. (9), it is evident that $\widehat{\mathbf{P}}_{k(-)}$ contains the unknown variable $\mathbf{u}_{k-1}^f$, which implies that the weights $\tilde{\mathbf{R}}_k$ in the WLS problem also contain an unknown variable. This makes the entire problem more complex and difficult to solve. It should also be noted that, based on Eq. (7) and Eq. (8), $\mathbf{u}_{k-1}^f$ is present not only in the first term of $\tilde{\mathbf{h}}\left(\tilde{\mathbf{x}}_k\right)$ but also in the second term $\widehat{\mathbf{x}}_{k(-)}$. Given that each iterative update of $\mathbf{u}_{k-1}^f$ has a modest impact on $\widehat{\mathbf{P}}_{k(-)}$, a simplification is applied to facilitate solving Eq. (13). Initially, the value of $\widehat{\mathbf{P}}_{k(-)}$ is calculated using the previously known $\mathbf{u}_{k-1}^f$ (or the measured value in the first iteration), thereby eliminating unknowns from the weights in the WLS problem. This transforms the problem into a standard WLS form, allowing a WLS solver to obtain an updated $\mathbf{u}_{k-1}^f$, which is then used to further update $\widehat{\mathbf{P}}_{k(-)}$. This process is iterated until convergence is achieved. Through this method, a stable solution to Eq. (13), which is otherwise difficult to solve directly, is gradually obtained.

5) Iterative solution. As the correction step of KF filtering has been expressed as a WLS problem (13), iterative optimization algorithms such as the Gauss-Newton method, the Levenberg-Marquardt algorithm, etc., can be used to solve it. In this paper, we present the Gauss-Newton method for solving (13), while other solution algorithms to nonlinear least squares problems can also be employed.

5.1) Set iteration number $j = 0$. Initialize the augmented state vector $\tilde{\mathbf{x}}_{j,k}$, set the state estimate tolerance $\tau > 0$, and bad data detection threshold $\kappa > 3$ corresponding to a confidence level of 99.74% [26].

5.2) Compute the Jacobian matrix and the gain matrix:

$$\tilde{\mathbf{H}}_{j,k}\left(\tilde{\mathbf{x}}_{j,k}\right) = \frac{\partial \tilde{\mathbf{h}}\left(\tilde{\mathbf{x}}_{j,k}\right)}{\partial \tilde{\mathbf{x}}_{j,k}}, \tag{14}$$

$$\tilde{\mathbf{G}}_{j,k}\left(\tilde{\mathbf{x}}_{j,k}\right) = \tilde{\mathbf{H}}_{j,k}^{T}\left(\tilde{\mathbf{x}}_{j,k}\right) \tilde{\mathbf{R}}_{j,k}^{-1} \tilde{\mathbf{H}}_{j,k}\left(\tilde{\mathbf{x}}_{j,k}\right). \tag{15}$$

There are two points to note here. Firstly, the predicted value of $\widehat{\mathbf{x}}_{k(-)}$ contains information about $\mathbf{u}_{k-1}^f$. Therefore, when computing the Jacobian matrix for the first subvector of $\tilde{\mathbf{h}}\left(\tilde{\mathbf{x}}_k\right)$, $\widehat{\mathbf{x}}_{k(-)}$ cannot be treated as a constant. Secondly, $\widehat{\mathbf{P}}_{k(-)}$ will be updated along with the update of $\mathbf{u}_{k-1}^f$, so here $\tilde{\mathbf{R}}_k$ is variable with the number of iterations j, denoted as $\tilde{\mathbf{R}}_{j,k}$.

5.3) Evaluate the augmented state update:

$$\Delta\tilde{\mathbf{x}}_{j,k} = \tilde{\mathbf{G}}_{j,k}(\tilde{\mathbf{x}}_{j,k})^{-1} \tilde{\mathbf{H}}_{j,k}^{T}\left(\tilde{\mathbf{x}}_{j,k}\right) \tilde{\mathbf{R}}_{j,k}^{-1} \left[\tilde{\mathbf{y}}_k - \tilde{\mathbf{h}}\left(\tilde{\mathbf{x}}_{j,.k}\right)\right]. \tag{16}$$

5.4) Update the augmented state vector:

$$\tilde{\mathbf{x}}_{j+1,k} = \tilde{\mathbf{x}}_{j,k} + \Delta\tilde{\mathbf{x}}_{j,k}. \tag{17}$$

5.5) Check the termination criterion. If $|\Delta\tilde{\mathbf{x}}_{j,k}| < \tau$ then set $\tilde{\mathbf{x}}_{k(+)} = \tilde{\mathbf{x}}_{j,k}$ and $\tilde{\mathbf{H}}_k = \tilde{\mathbf{H}}_{j,k}$, and go to step 6. Otherwise, set $j \leftarrow j+1$ and go to step 5.6.

5.6) As previously mentioned, utilize the updated $\mathbf{u}_{j,k-1}^f$ (a subvector of the augmented vector $\tilde{\mathbf{x}}_{j,k}$) to accomplish the prior prediction of the state variables $\widehat{\mathbf{x}}_{k(-)}$ and form the augmented vector according to Eq. (5) - Eq. (8) in step 3. At the same time the weights for the WLS problem, $\widehat{\mathbf{P}}_{k(-)}$

are recomputed according to Eq. (9) in step 3. Then go to step 5.2.

6) Update the posterior covariance matrix of the augmented state vector as follows:

$$\tilde{\mathbf{P}}_{k(+)} = \left(\tilde{\mathbf{H}}_k^T \tilde{\mathbf{R}}_{j,k}^{-1} \tilde{\mathbf{H}}_k\right)^{-1} = \tilde{\mathbf{G}}_k^{-1}. \tag{18}$$

7) Bad data detection and correction. When the error in a measurement exceeds the normal range of noise, it is deemed a gross error, and the data point is deemed *bad data*. Traditional DSE methods typically do not consider the possibility of bad data in inputs, only focusing on the possibility of bad data in the output. For example, Ref. [27] employs a combination of the robust exponential-absolute-value-based estimator and the UKF to mitigate the effects of bad data or outliers. Another example is the resilient estimator employed in Ref. [13] , which can also reduce the influence of outliers on the outputs. However, as discussed earlier, many input variables in power systems also originate from measurement devices all are telecommunicated, thus are also subject to gross errors. In order to detect and suppress bad data in both inputs and outputs, this paper implements the LNR method [28], [29].

7.1) Compute the residual covariance matrix:

$$\tilde{\mathbf{\Omega}}_k = \tilde{\mathbf{R}}_k - \tilde{\mathbf{H}}_k^T \left(\tilde{\mathbf{x}}_k\right) \tilde{\mathbf{P}}_{k(+)} \tilde{\mathbf{H}}_k \left(\tilde{\mathbf{x}}_k\right). \tag{19}$$

7.2) Compute the normalized residuals by dividing the absolute values of the residuals by the corresponding diagonal elements of the covariance matrix:

$$\tilde{\mathbf{r}}_k^N = \left(diag\left(\tilde{\mathbf{\Omega}}_k\right)\right)^{-\frac{1}{2}} \left(\tilde{\mathbf{y}}_k - \tilde{\mathbf{h}}\left(\tilde{\mathbf{x}}_{k(+)}\right)\right). \tag{20}$$

7.3) Find the input/output measurement corresponding to the largest normalized residual as follows:

$$u = \arg\max_j \left\{\left|\tilde{\mathbf{r}}_k^{jN}\right|\right\}, \tag{21}$$

where $\tilde{\mathbf{r}}_k^{jN}$ is the j^{th} element of $\tilde{\mathbf{r}}_k^N$.

7.4) If $\left|\tilde{\mathbf{r}}_k^{uN}\right| > \kappa$ then the u^{th} entry is deemed bad data and corrected as follows:

$$\tilde{\mathbf{y}}_k^u \leftarrow \tilde{\mathbf{y}}^u - \frac{\tilde{\mathbf{R}}_k^{uu}}{\tilde{\mathbf{\Omega}}_k^{uu}} \tilde{\mathbf{r}}_k^u, \tag{22}$$

then go back to step 5. Otherwise, go to step 8. When bad data is detected, removing the bad data of measurement and performing DSE is a common approach. In this paper, the correction method is used for ease of implementation, as it does not require modification of the dimensions of the measurement vector, measurement function vector, and Jacobian matrix. In practice, both the removal method and the correction method are technically acceptable. Another method for handling bad data is to de-weight it without correction, such that its impact on the DSE result is reduced. However, in our approach, the detected bad data is actively corrected until the magnitude of the error is in the range of regular noise. In this process, the measurement should keep the same weight (i.e., keeping the same error variance as regular noise) such that the hypothesis testing can be correctly performed.

8) Noise adaptation. In view of the fact that the statistics of input/output/process noise are typically unknown in power system applications, an adaptive estimation method based on covariance matching [30] is devised to obtain an approximate estimate of the noise distribution variances. Covariance matching can be divided into two types based on the information it uses: Residual-based Adaptive Estimation (RAE) and Innovation-based Adaptive Estimation (IAE) [30]. As the correction step is transformed into a WLS regression problem where the residuals are explicitly obtained, RAE is adopted in the proposed method. In addition, the residual data within a certain time window is used to to reduce errors.

8.1) Compute the covariance matrix of the augmented residuals as follows:

$$\mathbf{A}_k = \frac{1}{M} \sum_{j=k-M+1}^{k} \left(\tilde{\mathbf{y}}_j - \tilde{\mathbf{h}}\left(\tilde{\mathbf{x}}_{j(+)}\right)\right)^T \left(\tilde{\mathbf{y}}_j - \tilde{\mathbf{h}}\left(\tilde{\mathbf{x}}_{j(+)}\right)\right), \tag{23}$$

where M represents the length of the time window.

8.2) Compute the covariance matrix of the augmented noise as follows:

$$\tilde{\mathbf{R}}_{k(+)} = \mathbf{A}_k + \tilde{\mathbf{P}}_{k(+)}. \tag{24}$$

Based on Eq. (13), the posterior covariance matrices of measurement noise (i.e., the diagonal block of $\tilde{\mathbf{R}}_{k(+)}$ corresponding to actual measurements) and of process noise (i.e., the diagonal block of $\tilde{\mathbf{R}}_{k(+)}$ corresponding to states minus the prior covariance matrix $\widehat{\mathbf{P}}_{k(-)}$) can be extracted.

9) Go back to step 2.

In summary, this subsection outlines the specific process of the AICKF-UcI method. Addressing potential nonlinearity in the state transition and output equations, AICKF-UcI employs Cubature rule and iterative solving methods respectively. Furthermore, AICKF-UcI utilizes the LNR method to detect and correct bad data in the inputs and outputs, and employs an adaptive algorithm to update the covariance matrix of the noise. The flowchart of the algorithm is provided in Fig. 2.

C. Observability, Redundancy and Accuracy

If the complete set of the states of a system can be reconstructed from its outputs, then the system is considered observable. The observability of a dynamic system has been extensively studied. Ref. [31] provides some methods for assessing observability in both linear and nonlinear systems. Compared with conventional DSE methods wherein only the states are to be estimated, the AICKF-UcI framework increases the number of variables to be estimated (i.e., the UcIs); however, unlike UIs which are completely unknown and dependent on output measurements for inference, each UcI has its own direct measurement; hence, all the UcIs are always observable. In conclusion, including the estimation of UcIs will not turn an observable system into an unobservable one; in other words, *for a given dynamic system, as along as all the state variables are observable in the conventional KF framework where the inputs are assumed to be completely known, the system will remain observable in the proposed framework where the inputs are uncertain but with measurements.*

In addition to observability, the information redundancy can also be analyzed, which is defined as the ratio of the number of independent equations that can be used to infer unknown

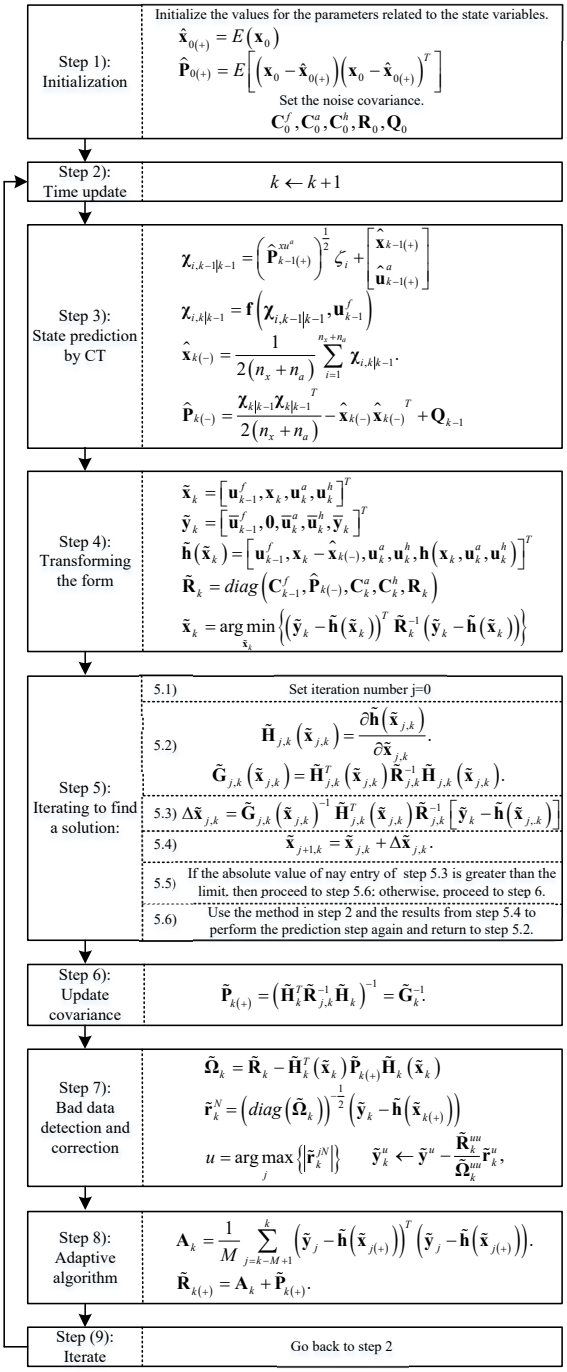

Fig. 2. The flowchart of proposed AICKF-UcI.

variables to the number of unknown variables. Obviously, any observable system must have a redundancy level that is greater than 1. The higher the redundancy level, the better the noise filtering and bad data processing capabilities. In the conventional KF framework with inputs are completely known, the goal is to estimate the state vector with a dimension of n_x, while there are n_x state transition equations and n_y output equations. Hence, at each particular time step, the redundancy level is $(n_y + n_x)/n_x > 1$. A larger number of n_y leads to a higher redundancy level. For AICKF-UcI, due to the recognition of the imperfection of input variables, the number of variables to be estimated is increased. In addition to the n_x state variables, we also need to estimate $n_f + n_h + n_a$ external inputs simultaneously. At the same time, since these inputs are obtained through measurements, $n_f + n_h + n_a$ measurement equations are suplemented. Therefore, one has $(n_y+n_x)/n_x > (n_y+n_x+n_f+n_h+n_a)/(n_x+n_f+n_h+n_a) > 1$, namely, the redundancy level is reduced due to the imperfection of input variables, yet it is still greater than the critical level of 1.

Another aspect that needs to be discussed is the accuracy of DSE results. Both qualitative and quantitative analyses can be performed by examining the augmented gain matrix $\tilde{\mathbf{G}}_{j,k}$ shown in Eq. (25) (For the sake of brevity, we have omitted the subscript 'k' for the covariance matrix and moved the superscripts that represent different variables, such as 'a' and 'h', to subscripts).

Examining the diagonal blocks of the matrix in Eq. (25), each diagonal block exhibits a form similar to the innovation (or the so-called pre-fit residual) covariance in the traditional KF framework. Quantitative analysis can be performed by computing the inverse of matrix $\tilde{\mathbf{G}}_{j,k}$, which yields the covariance matrix of the errors in the estimates of all the variables. However, a qualitative analysis that examines the structures of the diagonal blocks can provide very useful insights as well. Taking the accuracy of $\mathbf{u}_{k-1}^f$ as an example, $\mathbf{C}_f^{-1}$ represents the contribution of the measurements of $\mathbf{u}_{k-1}^f$ itself, while $\mathbf{F}_f^T\hat{\mathbf{P}}^{-1}\mathbf{F}_f^T$ represents the contribution of the inference based on the state transition equations. When $\mathbf{F}_f^T$ is small, the estimation result will rely more on the measurements of the UcIs themselves, whereas, a larger $\mathbf{F}_f^T$ will make the estimation more dependent on the inference based on the state transition equations. A practical example of the former case is when the discretization of (1) takes a very small time step length (as is the often case of the DSE of IBRs), where the estimation of $\mathbf{u}_{k-1}^f$ can be relatively inaccurate unless its own measurement is of very high quality. This will be demonstrated in the case 1 of Section III.

III. Simulation Results

To validate the performance of AICKF-UcI, this section will present simulation results on three different test cases: a virtual dynamic system, a PMSG in the IEEE 34-node test feeder, and a SG in the New England 68-bus test system.

A. DSE of a Virtual Dynamic System

The three types of inputs in Eq. (4) may not all exist in the objects of the power system that actually require DSE (such as SG, IBR, etc.). Therefore, to demonstrate the algorithm's versatility to handle systems with all three types of UcIs in Eq. (4), i.e., $\mathbf{u}^a$, $\mathbf{u}^f$, $\mathbf{u}^h$, a virtual dynamic system is designed, as shown in Fig. 3.

Suppose there is a wooden block with a mass of m fixed in a wind tunnel using a spring with an elastic constant r. The wooden block experiences an external tension force F and, at the same time, experiences air resistance. The air resistance is proportional to the square of the relative velocity between the block and the air, with a proportionality coefficient of n. As a result, we have two state variables, which are the

$$\tilde{\mathbf{G}}_{j,k}\left(\tilde{\mathbf{x}}_{j,k}\right)=\tilde{\mathbf{H}}_{j,k}^{T}\left(\tilde{\mathbf{x}}_{j,k}\right)\tilde{\mathbf{R}}_{j,k}^{-1}\tilde{\mathbf{H}}_{j,k}\left(\tilde{\mathbf{x}}_{j,k}\right)$$
$$=\begin{bmatrix}\mathbf{C}_f^{-1}+\mathbf{F}_f^T\hat{\mathbf{P}}^{-1}\mathbf{F}_f^T & -\mathbf{F}_f^T\hat{\mathbf{P}}^{-1} & \mathbf{0} & \mathbf{0}\\ -\hat{\mathbf{P}}^{-1}\mathbf{F}_f^T & \hat{\mathbf{P}}^{-1}+\mathbf{H}_x^T\mathbf{R}^{-1}\mathbf{H}_x & \mathbf{H}_x^T\mathbf{R}^{-1}\mathbf{H}_a & \mathbf{H}_x^T\mathbf{R}^{-1}\mathbf{H}_h\\ \mathbf{0} & \mathbf{H}_a^T\mathbf{R}^{-1}\mathbf{H}_x & \mathbf{C}_a^{-1}+\mathbf{H}_a^T\mathbf{R}^{-1}\mathbf{H}_a & \mathbf{H}_a^T\mathbf{R}^{-1}\mathbf{H}_h\\ \mathbf{0} & \mathbf{H}_h^T\mathbf{R}^{-1}\mathbf{H}_x & \mathbf{H}_h^T\mathbf{R}^{-1}\mathbf{H}_a & \mathbf{C}_h^{-1}+\mathbf{H}_h^T\mathbf{R}^{-1}\mathbf{H}_h\end{bmatrix} \quad (25)$$

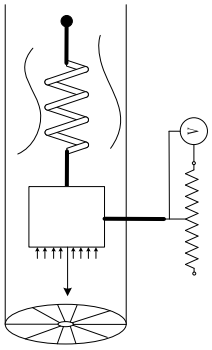

Fig. 3. Hypothetical experiment: a wooden block in a wind tunnel.

relative position (x_p) and velocity (x_s) of the wooden block, to estimate. The state transition equations involve two inputs, namely the tension force u_F and the wind speed u_w:

$$\begin{cases}\frac{dx_p}{dt}=x_s,\\ \frac{dx_s}{dt}=\frac{1}{m}\left(u_F+mg-rx_p-n(u_w+x_s)^2\right).\end{cases} \quad (26)$$

This virtual dynamic system has two measurements. One is a sensor on the wooden block measuring the relative velocity between the block and the spring (z_s), and a rigidly linked sliding rheostat measuring the current (z_I) through an external voltage (u_V). The output equations are as follows:

$$\begin{cases}y_I=\frac{u_V}{r_0+x_p},\\ y_s=u_w+x_s.\end{cases} \quad (27)$$

In this system, u_F only exists in the state transition equation, u_V only exists in the output equation, and u_w simultaneously exists in both. *It is a simple and small system but with all three types of external inputs present in (4).*

To perform DSE, independent Gaussian white noise is added as process noise and measurement noise, with standard deviations of 0.0026 and 0.1, respectively. The Standard Devitations (SDs) of the noises in inputs u_w, u_v, and u_F are 0.5, 0.5, and 1, respectively. The sampling frequency is 240Hz. Three widely-known baseline methods, CKF, IEKF, and EKF-UI, are performed along with the proposed AICKF-UcI method.

1) State estimation result: For the purpose of comparison, all $\mathbf{Q}$ and $\mathbf{R}$ values used in the DSE methods are set to their true values. From Fig. 4 (a) and (b), it can be observed that, using the Root Mean Square Error (RMSE) as a metric, the AICKF-UcI method consistently achieves superior results compared to the other methods. In Fig. 4 (b), it can be observed that that EKF-UI, as a typical method of the xKF-UI framework, produces much higher state estimation errors than the proposed method. This is because it adds an input

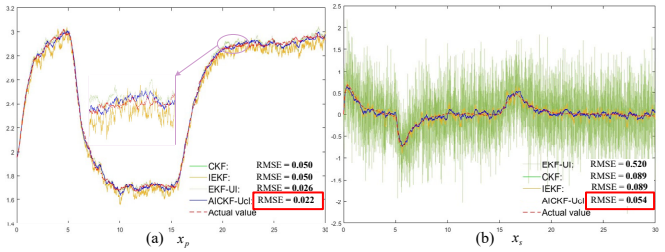

Fig. 4. State estimation results under UcIs.

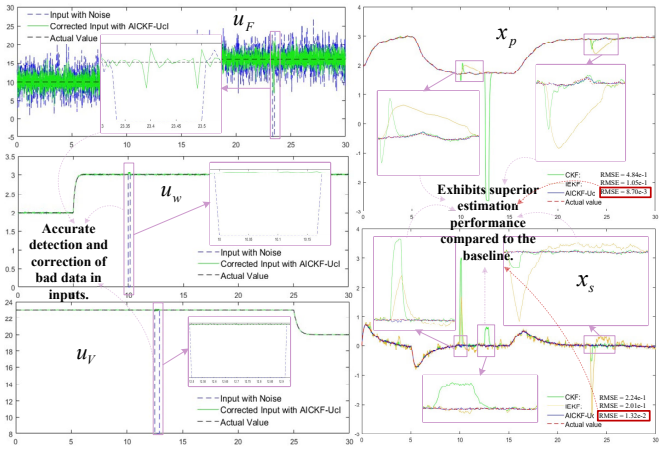

Fig. 5. Bad data detection and correction of input variables.

variable to be estimated without the introduction of additional information, leading to a drastic declination of information redundancy. The proposed method, on the other hand, further incorporates measurements of inputs as additional information, leading to enhanced information redundancy and estimation accuracy compared with the conventional xKF-UI framework.

2) Bad data detection and correction: In this experiment, bad data are intentionally introduced into the input variables as follows: From 10s to 10.67s, the measurement of u_w becomes 0; measurement anomalies. From 12.5s to 12.92s and 23.33s to 23.5s, u_V and u_F are set to 8 and -5, respectively.

The traditional CKF and IEKF methods, both integrated with the LNR test for the bad data detection and correction, are taken as baselines for comparison. The results are shown in Fig. 5 and Fig. 6. AICKF-UcI successfully achieves the detection and correction of bad data in input variables and maintains high accuracy of state estimation. *The traditional methods falsely blame the bad data in the input variables on the output variables, leading to incorrect output corrections and deterioration of state estimation accuracy.* This is due to their underlying assumption of precise inputs and inability to inspect gross errors in input variables.

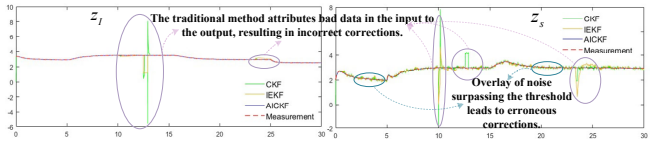

Fig. 6. Traditional methods' mistaken corrections of outputs in the presence of bad data in inputs.

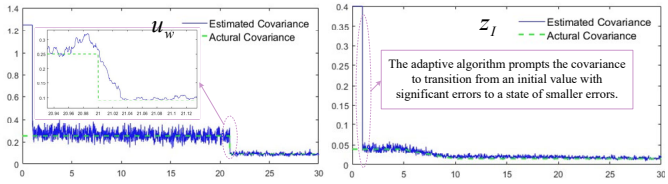

Fig. 7. Variance estimation results of some inputs and outputs.

3) Noise adaptation: The condition of unknown variances of input, output, and process noise distributions is also tested. Simulation results shown in Fig. 7 validates that the adaptive algorithm effectively drives the covariance estimates of the noise close to the true values.

In the simulation tests, the length of time window M is set to 128 (equivalent to two fundamental waveform cycles). The standard deviation of the input signal u_w noise is abruptly changed at 21s, becoming 60% of the previous one (resulting in the covariance changing to 36%). The standard deviation of the output measurement noise z_I is gradually reduced starting at 5s, reaching 60% of the previous value at 10s and then remaining constant. As seen in Fig. 7, whether the standard deviation of the noise changes abruptly or gradually, the method can accurately track the changes in noise covariance when a time window of 128 points is used. Furthermore, when zooming in on the tracking of u_w at 21s, it can be observed that the adaptive algorithm effectively converges to the new covariance within approximately 34 ms, which aligns with expectations.

4) Estimation results of inputs in the state transition equations: This subsection studies the estimation of input variables that appear in state transition equations, which are very common in power systems. As analyzed in Section II-C, different values of $\mathbf{F}_f$ will affect the accuracy of the estimation. In the process of converting continuous differential equations into difference equations, longer discretization step length leads to higher values of $\mathbf{F}_f$, which helps increase the accuracy of input estimation. To verify this observation, all other conditions are kept constant, and only the sampling frequency is varied in this experiment. The advantages of AICKF-UcI and the influence of sampling frequency on xKF-UI will be concurrently assessed.

The estimation results at a sampling frequency of 240Hz are shown in Fig. 8 (a). The RMSE of the EKF-UI results is even larger than that of the measurement. AICKF-UcI produces the most accurate estimation results. Furthermore, if we further increase the sampling frequency, EKF-UI fails to converge. Upon reducing the sampling frequency (i.e., increasing the discretization step length), as depicted in Fig. 8 (b), the estimation accuracies of both methods are considerably improved as expected. Again, the RMSE of the proposed

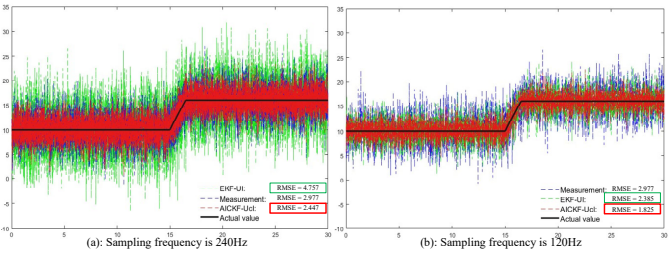

(a): Sampling frequency is 240Hz (b): Sampling frequency is 120Hz

Fig. 8. Estimation results of inputs in the state transition equations.

AICKF-UcI method remains consistently lower than that of the EKF-UI method.

While high sampling frequencies (short sampling intervals) can decrease the accuracy of input estimation, excessively low sampling frequencies (long time intervals) bring additional challenges, for example, increased discretization errors of nonlinear systems, reducing the precision of DSE results. Therefore, for DSE involving UcI or UI in the state transition equations, an appropriate sampling frequency that is neither too high nor too low must be selected.

B. DSE of a PMSG in a Power Distribution System

Through the experiments in the virtual dynamic system with all three types of input structures, we have gained insights into the performance of the AICKF-UcI algorithm in all aspects. Next, it will be validated in actual power system test cases.

In this section, DSE is performed on a PMSG wind turbine connected to the IEEE 34-node test feeder, illustrated in Fig. 9. The rated capacity of the PMSG is 1.2 MVA. Additionally, PV systems, energy storage systems, and dynamic loads are integrated into the grid to represent an comprehensive active distribution system. The disturbances to the PMSG primarily stem from fluctuations in the wind speed. The state transition equations of the PMSG are illustrated in Fig. 9. The wind speed of the PMSG begins to increase from 8 m/s at 2s, reaching 9.5 m/s at 2.4s, and remains stable until the end of the simulation. The transmission system experiences a voltage change at 3.5s. The voltage drops from the initial 1.05 p.u. to 1.0 p.u. at 3.6s, and then stabilized for the remainder of the simulation.

The output variables are the mechanical rotational speed of the PMSG, ω_m^z; dq-axis currents on the PMSG side, I_{sd}^z and I_{sq}^z; the voltage of the DC-link capacitor, V_{DC}^z; the active power output to the grid, P_g^z.

Based on the proposed framework, the input variables can be categorized as follows: the wind speed v_w^{ex} and the four control signals V_{id}^c, V_{iq}^c, V_{gd}^c and V_{gq}^c solely influence the state transition equations, thus forming $\mathbf{u}^f$. V_{gd}^{ex} and V_{gq}^{ex} influence both state transition equations and output equations, thus forming $\mathbf{u}^a$. There is no output categorized into $\mathbf{u}^h$.

In the DSE of the PMSG, the dynamic model account for the electro-magnetic transients of inductors and capacitors, so Point-of-Wave (PoW) measurements are directly used by the DSE. The sampling frequency of measurements is set as 480Hz, which is down-sampled from PoW measurements provided by PMSG sensors, whose sampling rates are typically

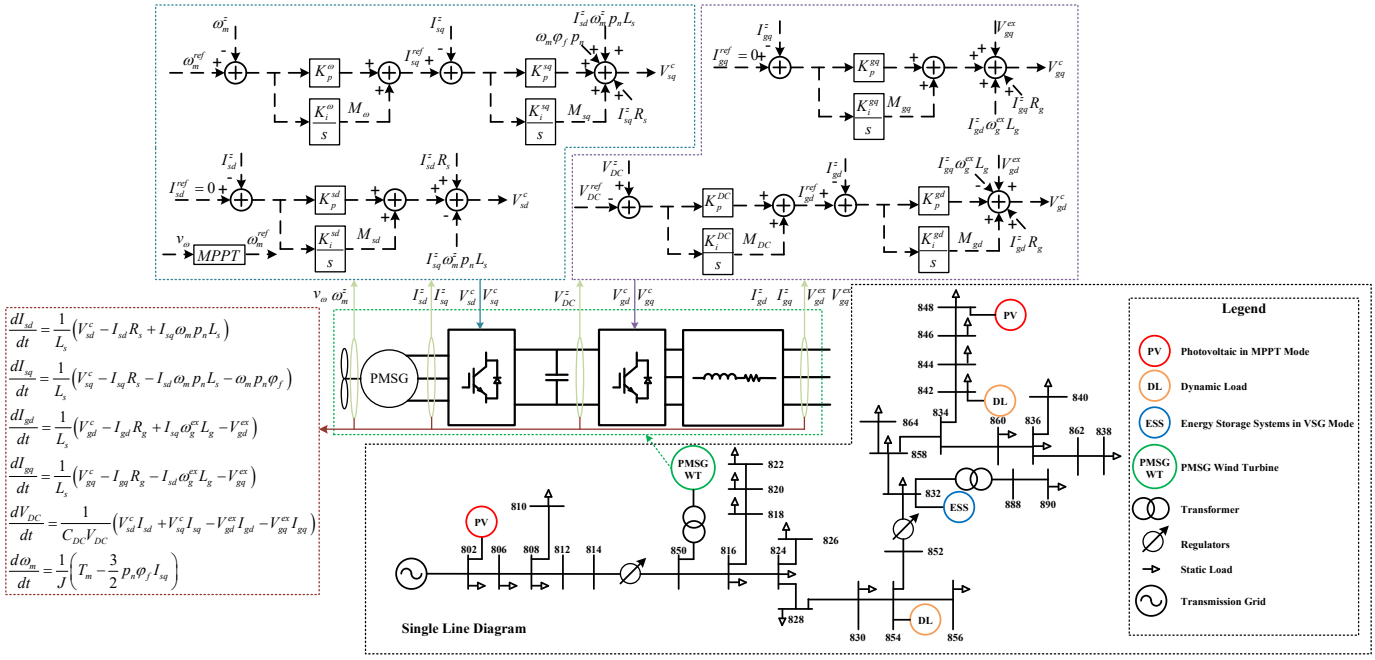

Fig. 9. PMSG control block diagram and related equations in the IEEE 34-node test feeder.

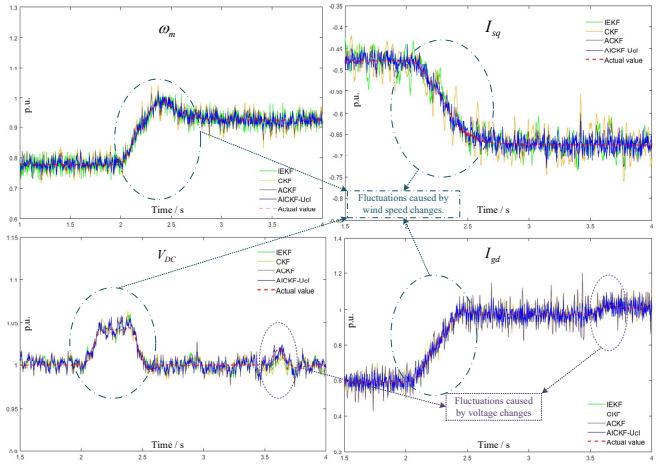

Fig. 10. State estimation results under UcIs.

thousands of kilo Hertz. Taking into account the relatively limited accuracy of measurement devices in the distribution system and the challenge of accurately measuring wind speed, the standard deviations of input noise are as follows: The wind speed v_w^{ex} from lower-precision measurement devices is set to 10%, while the remaining electrical quantities from the same measurement devices are set to 2%.

1) State estimation result: Three methods were chosen as baselines, namely IEKF, CKF, and ACKF. Due to the poor performance of the IEKF-UI (low accuracy and numerical stability) observed in Case 1, it is not included in the baseline methods for comparison. To test the performance under unknown noise statistics, the initial measurement noise covariance estimate is set to four times the true value. Some results are shown in Fig. 10, and the RMSE of different methods are shown in Table I.

TABLE I
THE RMSE OF DIFFERENT DSE METHODS.

	AICKF-UcI	ACKF	IEKF	CKF
ω_m	**1.32%**	1.85%	1.90%	2.44%
I_{sd}	**1.24%**	1.35%	2.22%	2.13%
I_{sq}	**1.45%**	1.76%	2.35%	3.07%
I_{gd}	**3.02%**	4.99%	3.50%	3.54%
I_{gq}	7.03%	9.78%	6.04%	6.01%
V_{DC}	**0.54%**	0.70%	0.62%	0.70%

From the results, it can be observed that compared to CKF, ACKF improves estimation accuracy for DSE of ω_m, I_{sd} and I_{sq}. When comparing two methods for handling nonlinear systems, IEKF and CKF, no significant differences are observed. Therefore, only CKF is selected as the baseline for further comparison. On the other hand, the AICKF-UcI method exhibits significantly higher accuracy than all baseline methods for all state variables except I_{gq} with a similar of RMSE. The results verifies that the by explicitly considering the uncertainty of inputs, the proposed method can achieve better filtering performance compared with conventional methods that do not explicitly model and filter noise in inputs.

In terms of computation time, EKF-UI is the shortest, at 0.033s; followed by IEKF at 0.12s; CKF at 0.23s; and AICKF-UcI at 0.68s as well as the noise adaptation capabilities. However, it is still much faster than real time (estimating the trajectory of 4s takes 0.68s, which means that at a sampling/reporting frequency of 480 Hz, completing 1920 DSEs over 4s requires only 0.68s, with an average of just 0.35 ms per DSE.), indicating its satisfactory capability of real-time applications. Note that the proposed DSE method is designed for a distributed estimation scheme where each estimator only tracks the state of an individual dynamic component of a power system, so the dimension of the dynamic system modeled by

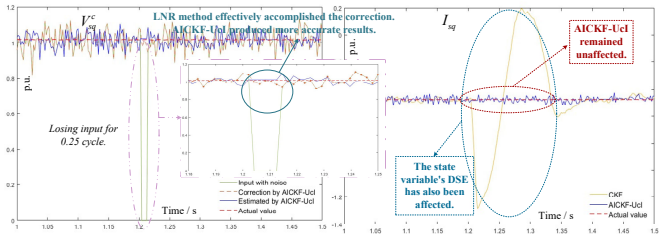

Fig. 11. State estimation results in the presence of bad data in the inputs.

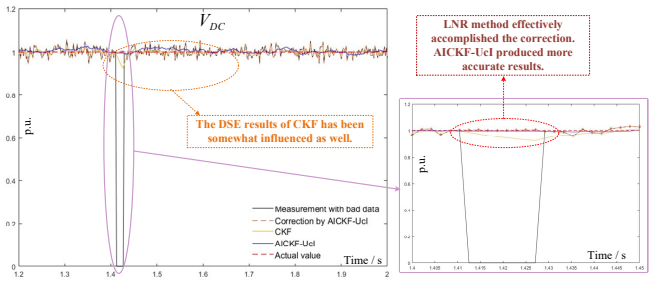

Fig. 12. State estimation results in the presence of bad data in the outputs.

the DSE is moderate. Given that PMSG is a relatively complex component, and this simulation also examines a relatively demanding case where the DSE adopts an EMT model and intakes PoW measurements with a much higher frequency than that of phasor-domain PMU measurements, the fact that the DSE works well for this case is a good indication that it is likely to satisfy the real-time computational requirements of all potential use cases of the proposed DSE.

2) Bad data detection and correction: As traditional methods assume that input information is reliable, bad data detection and correction are only for processing outputs (conventionally-defined "measurements"). Therefore, bad data in input variables are attributed to abnormalities of the measurements of output variables, leading to incorrect correction actions. Additionally, input noise can interfere with the LNR statistical test, resulting in erroneous outcomes. To validate the robustness of the proposed AICKF-UcI algorithm against bad data in input variables, two experiments are conducted.

First, it is assumed that at 1.2s, due to communication anomalies or a cyber attack, V_{sq}^{c} from the controller (an input of the PMSG system) becomes 0 and lasts for 0.25 cycle. The DSE results are depicted in Fig. 11. The proposed method accurately identifies and corrects the erroneous input signal, and the accuracy of state estimation is maintained. In contrast, for the traditional CKF method, there are significant deviations in the state estimates.

Next, we consider the scenario where bad data is present in the output variables (conventionally-defined "measurements"). At 1.41s, due to sensor anomalies, the measured value of the PMSG output, V_{DC}^{z} becomes 0 and lasts for half a cycle. The results of DSE are shown in Fig. 12. Similar with the situation where bad data exists in the inputs, the LNR method effectively detects and corrects the bad data in the outputs. Therefore, it can be concluded that the proposed method can clearly distinguish gross errors in input variables and those in output variables, a unique capability that conventional methods do not have.

C. DSE of an SG in a Power Transmission System

Finally, the proposed AICKF-UcI framework is validated on an SG in the 68-bus 16-machine test system, which is based on a reduced-order equivalent model of the New England test system (NETS) and New York power system (NYPS) [24], shown in Fig. 13.

An SG is modeled by a set of sixth-order differential equations, where $E_d^{'}$ and $E_q^{'}$ represent transient EMF due to the flux in q-axis damper coil and field flux linkages; φ_d and φ_q represent subtransient EMFs due to the fluxes d and q axes damper coils, respectively; ω and δ represent the rotor speed and angle, respectively. For the parameters, $x_d^{''}$, $x_d^{'}$, and x_d refer to the d-axis subtransient reactance, transient reactance and synchronous reactance, respectively; $T_{d0}^{''}$ and $T_{d0}^{'}$ represent d-axis subtransient time constant and transient time constant, respectively. The subscript q indicates q-axis parameters. x_{ls} is the armature leakage reactance and J is the inertia coefficient. V_d, V_q, I_d and I_q represent the voltage and current in d and q axis, respectively. All the data are in per unit values.

The inputs of the state transition equation include the input torque T_m provided by the governor, the excitation voltage E_{fd} supplied by the excitation system, and the current phasor I_r and I_i (representing the real part and the imaginary part respectively) obtained through PMU. The system output is the terminal voltage phasor V_r and V_i (representing the real part and the imaginary part respectively) obtained through a PMU. At 1s, a three-phase-to-ground fault occurs along line 54, and at 1.18s, the faulted line is disconnected. The DSE is performed for SG 1. The reporting rate of the PMU is 120 frames per second, meeting IEEE standard requirements [32].

Ref. [24] employs the UKF method and incorporates the influence of inputs through an augmented matrix in both the prediction and update steps. It demonstrates improved estimation results under conditions of relatively low noise levels. Since the comparison between AICKF-UcI and various methods under higher noise has already been validated in the PMSG case, in this experiment we opt for a situation similar to that in Ref. [24]. Considering the use of PMUs as measurement devices in the transmission system, it is reasonable to assume that the measurements have relatively small errors under normal conditions. In this case, the performances of different DSE methods do not make a significant impact. As shown in Figs. 14 and 15, when there is no gross error in the measurements (either input or output), traditional CKF yields very satisfactory estimation results. This also indicates that the traditional approach of not considering input noise in DSE for SG has some validity. However, gross errors still exist due to issues such as the lack of calibration, loss of GPS signals, communication disruptions, and cyber attacks, which pose severe threats to DSE applications. *Notably, these gross errors can potentially appear in the output as well as in the input as both voltage phasors (outputs) and current phasors (inputs) are measured by PMUs.* This will cause problems for conventional DSE methods as they do not have

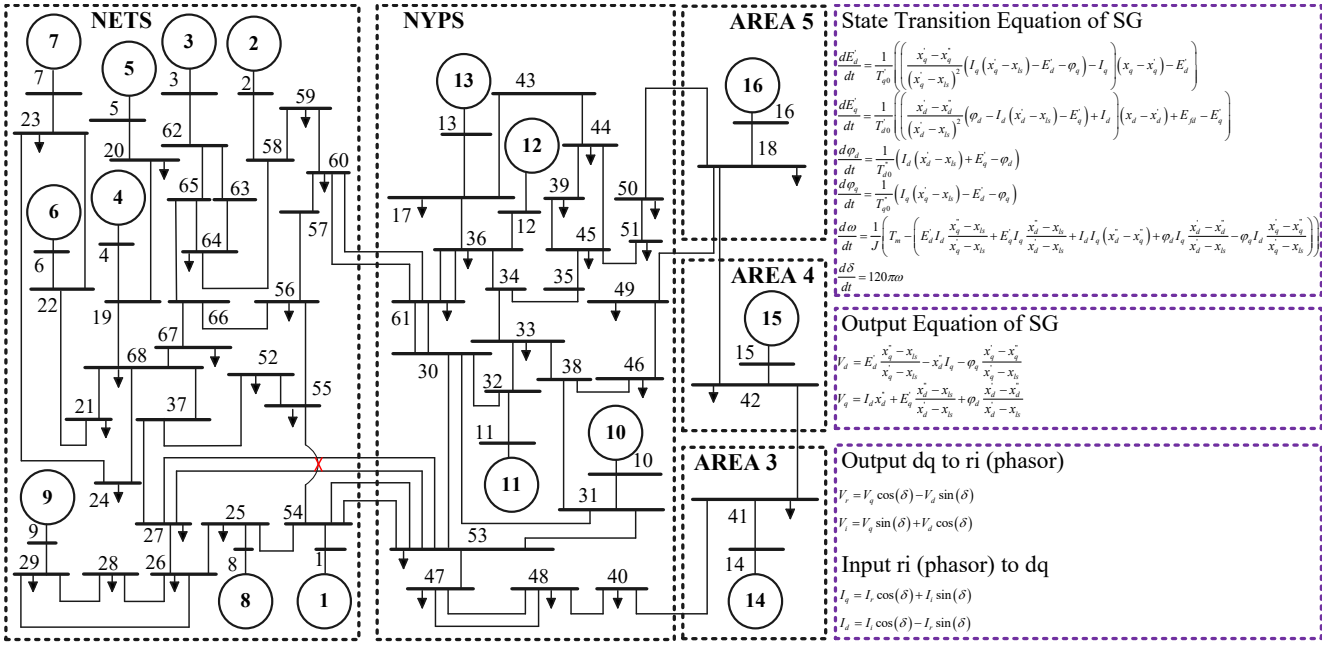

Fig. 13. 68-bus 16-machine test system and the SG dynamical model.

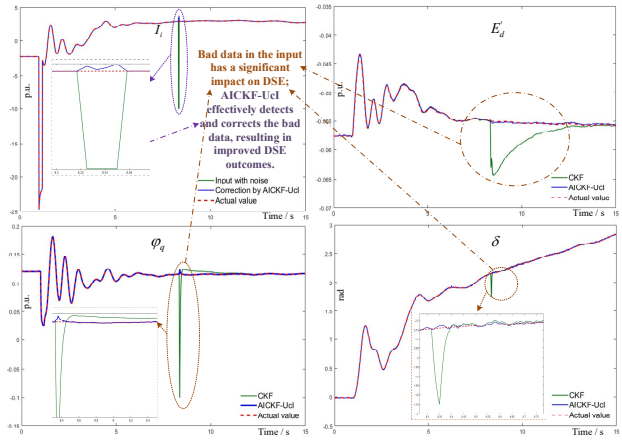

Fig. 14. State estimation results in the presence of bad data in I_i.

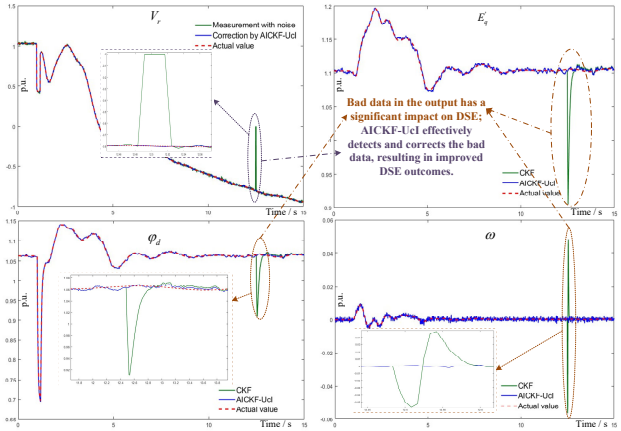

Fig. 15. State estimaton results in the presence of bad data in V_T.

TABLE II
THE RMSE OF DIFFERENT DSE METHODS FOR SG.

	$E_d^{'}$	$E_q^{'}$	φ_d	φ_q	ω	δ
AICKF-UcI	0.12‰	2.1‰	2.3‰	0.47‰	0.76‰	6.3‰
CKF	0.14‰	2.1‰	2.3‰	0.47‰	0.76‰	6.26‰
AICKF-UcI in BD	0.48‰	2.1‰	2.2‰	0.7‰	0.78‰	6.5‰
CKF in BD	2.1‰	3.8‰	2.5‰	9.6‰	1.6‰	17.7‰

the capability of inspecting bad data for inputs as they do for outputs. Meanwhile, a unique advantage of AICKF-UcI is that it can explicitly identify and correct bad data in the input signals caused by various reasons, thereby reducing the impact of gross errors in input variables on the estimation results. Therefore, the focus of this test case is on the detection and correction of bad data in input variables.

Given that electrical measurements for SGs are typically taken using PMUs, which provide accurate measurements even during significant changes in electrical quantities due to faults, the standard deviation of noise for electrical quantities is set to 1%, while the noise standard deviation for torque and excitation voltage is set to 10%.

In this case, we take the CKF as the baseline for comparison, as it has similar performance with ACKF in the case when the noise level is low. Suppose that at 8.325s, I_i experiences bad data, becoming -10, and persists for two cycles. From the results shown in Fig. 14, it can be observed that traditional DSE methods like CKF, which do not estimate and inspect the inputs, are significantly affected by the presence of bad data in the inputs. By contrast, the AICKF-UcI method effectively detects and corrects bad data in the inputs, thereby tracking the true state trajectory very closely even in the presence of bad data in system inputs. The RMSE results, as shown in Table II, clearly indicate that when there is no bad data in the input, the proposed method performs consistently with the traditional CKF method. However, when bad data is present in the input, as illustrated in the figures, the performance of AICKF-

TABLE III
DETECTION RATES OF THE LNR METHOD UNDER DIFFERENT BIASES.

Bias (±)	4.0σ	4.5σ	5.0σ	5.5σ	6.0σ	6.5σ	7.0σ
Detection Rate	17%	24%	49%	66%	78%	87%	95%
Bias (±)	8.0σ	9.0σ	10.0σ	12.0σ	15.0σ	20.0σ	30.0σ
Detection Rate	99%	100%	100%	100%	100%	100%	100%

UcI only slightly decreases, whereas the traditional method, lacking joint estimation of the inputs, results in significant errors.

In addition, we also verify the detection and correction capabilities of AICKF-UcI when bad data is present in the outputs. We assume that at 12.5s, V_r becomes 0 due to an abnormal operating condition of the PMU. As demonstrated by the results shown in Fig. 15, the LNR method is also capable of effective detection and correction when bad data is present in the outputs. Overall, the simulation results shown in Figs. 14 and 15 demonstrate the proposed method's unique capability of distinguishing between gross errors in input and output variables. This is a highly desirable feature for systems like SGs where both inputs and outputs come from PMU measurements and are prone to corruptions.

To validate the detection capability of the LNR method, 10 random V_r measurements are selected between 14s to 15s, and biases with a given magnitude are added to these measurements, which already contain noise. This simulation with 10 bad data points is repeated 10 times, effectively generating 100 different instances of bad data. The detection rate of bad data is evaluated on these 100 instances of bad data that are randomly selected but with the same magnitude of bias. Then, this whole process is repeated with different magnitudes of biases, gradually increasing from 4σ (which means 4 times the standard deviation) to 30σ. With the threshold κ set to 5, meaning that deviations exceeding 5 times the standard deviation are considered bad data, the detection rates under different magnitudes of biases are shown in Table III. It is observed that when the bias reaches 9σ, the detection rate reaches 100%.

Ten simulations of the AICKF-UcI without any bad data are repeated, and it is found that completing a 15s simulation takes an average of 0.4922s per run, which means that at a sampling/reporting frequency of 120 Hz, completing 1800 DSEs over 15s requires only 0.4922s, with an average of just 0.27 ms per DSE. Subsequently, ten simulations of the AICKF-UcI with ten bad data points, each with a 10σ bias, are repeated, and it is observed that completing a 15s simulation takes an average of 0.4944s per run. The results show almost no difference between the two, as the additional loops required by the LNR method after detecting bad data are very limited and do not impose a significant computational burden. This demonstrates that the computational efficiency of proposed method meets the real-time performance requirements for practical DSE of SGs.

IV. CONCLUSION

Traditional DSE methods focus on the noise filtering and bad data processing of output variables (conventionally-defined "measurements"), and treat input variables as either precisely known or completely unknown. Considering that in power systems, input signals are often obtained through measurement and/or telecommunication as well, this paper focuses on addressing situations where inputs are uncertain, i.e., with available information that may carry noise or gross errors. The proposed AICKF-UcI method aims at the joint estimation of inputs and states by adaptively filtering uncertain input information in nonlinear power systems.

Simulations are first carried out in a virtual system, which included all three types of input structures, to verify the effectiveness of the proposed method. Then, DSE tests are carried out on a PMSG in the IEEE 34-node test feeder and on an SG in the New England 68-bus 16-machine test system. These tests validate the versatility and reliability of the AICKF-UcI method for applications ranging from IBRs to SGs, and from distribution systems to transmission systems. Results show that the proposed method can 1) achieve high state estimation accuracy in the presence of substantial input noise, 2) distinguish between and suppress the impact of bad data in inputs and outputs, and 3) estimate the unknown statistics of various noise and enhance filtering performance. These features are highly desirable for many DSE applications where inputs may be corrupted in the complicated measurement and communication environment of power systems.

REFERENCES

[1] F. Aminifar, M. Shahidehpour, M. Fotuhi-Firuzabad, and S. Kamalinia, "Power system dynamic state estimation with synchronized phasor measurements," *IEEE Transactions on Instrumentation and Measurement*, vol. 63, no. 2, pp. 352–363, 2014.

[2] L. Fan and Y. Wehbe, "Extended kalman filtering based real-time dynamic state and parameter estimation using pmu data," *Electric Power Systems Research*, vol. 103, pp. 168–177, 2013.

[3] L. Dang, W. Wang, and B. Chen, "Square root unscented kalman filter with modified measurement for dynamic state estimation of power systems," *IEEE Transactions on Instrumentation and Measurement*, vol. 71, pp. 1–13, 2022.

[4] A. Sharma, S. C. Srivastava, and S. Chakrabarti, "A cubature kalman filter based power system dynamic state estimator," *IEEE Transactions on Instrumentation and Measurement*, vol. 66, no. 8, pp. 2036–2045, 2017.

[5] M. Huang, Z. Wei, J. Zhao, R. A. Jabr, M. Pau, and G. Sun, "Robust ensemble kalman filter for medium-voltage distribution system state estimation," *IEEE Transactions on Instrumentation and Measurement*, vol. 69, no. 7, pp. 4114–4124, 2020.

[6] G. G. Rigatos, "Particle filtering for state estimation in nonlinear industrial systems," *IEEE Transactions on Instrumentation and Measurement*, vol. 58, no. 11, pp. 3885–3900, 2009.

[7] C. Wang, Z. Qin, Y. Hou, and J. Yan, "Multi-area dynamic state estimation with pmu measurements by an equality constrained extended kalman filter," *IEEE Transactions on Smart Grid*, vol. 9, no. 2, pp. 900–910, 2016.

[8] Y. Wang, Z. Yang, Y. Wang, V. Dinavahi, J. Liang, and K. Wang, "Robust dynamic state estimation for power system based on adaptive cubature kalman filter with generalized correntropy loss," *IEEE Transactions on Instrumentation and Measurement*, vol. 71, pp. 1–11, 2022.

[9] W. Ma, C. Wang, L. Dang, X. Zhang, and B. Chen, "Robust dynamic state estimation for dfig via the generalized maximum correntropy criterion ensemble kalman filter," *IEEE Transactions on Instrumentation and Measurement*, vol. 72, pp. 1–13, 2023.

[10] J. Zhao, M. Netto, and L. Mili, "A robust iterated extended kalman filter for power system dynamic state estimation," *IEEE Transactions on Power Systems*, vol. 32, no. 4, pp. 3205–3216, 2017.

[11] F. Alonge, F. D'Ippolito, and A. Sferlazza, "Sensorless control of induction-motor drive based on robust kalman filter and adaptive speed estimation," *IEEE Transactions on Industrial Electronics*, vol. 61, no. 3, pp. 1444–1453, 2014.

[12] V. Stojanovic, S. He, and B. Zhang, "State and parameter joint estimation of linear stochastic systems in presence of faults and non-gaussian noises," *International Journal of Robust and Nonlinear Control*, vol. 30, no. 16, pp. 6683–6700, 2020.
[13] Y. Wang, Z. Yang, Y. Wang, Z. Li, V. Dinavahi, and J. Liang, "Resilient dynamic state estimation for power system using cauchy-kernel-based maximum correntropy cubature kalman filter," *IEEE Transactions on Instrumentation and Measurement*, vol. 72, pp. 1–11, 2023.
[14] E. Ghahremani and I. Kamwa, "Dynamic state estimation in power system by applying the extended kalman filter with unknown inputs to phasor measurements," *IEEE Transactions on Power Systems*, vol. 26, no. 4, pp. 2556–2566, 2011.
[15] S. Das and B. K. Panigrahi, "A pmu-based data-driven approach for enhancing situational awareness in building a resilient power systems," *IEEE Transactions on Industrial Informatics*, vol. 18, no. 7, pp. 4773–4784, 2022.
[16] G. Anagnostou, L. P. Kunjumuhammed, and B. C. Pal, "Dynamic state estimation for wind turbine models with unknown wind velocity," *IEEE Transactions on Power Systems*, vol. 34, no. 5, pp. 3879–3890, 2019.
[17] M. Zhu, H. Liu, J. Zhao, B. Tan, T. Bi, and S. S. Yu, "Dynamic state estimation for dfig with unknown inputs based on cubature kalman filter and adaptive interpolation," *Journal of Modern Power Systems and Clean Energy*, 2023.
[18] J. Zhao, Z. Zheng, S. Wang, R. Huang, T. Bi, L. Mili, and Z. Huang, "Correlation-aided robust decentralized dynamic state estimation of power systems with unknown control inputs," *IEEE Transactions on Power Systems*, vol. 35, no. 3, pp. 2443–2451, 2019.
[19] S. A. Nugroho, A. F. Taha, and J. Qi, "Robust dynamic state estimation of synchronous machines with asymptotic state estimation error performance guarantees," *IEEE Transactions on Power Systems*, vol. 35, no. 3, pp. 1923–1935, 2019.
[20] J. Zhao and L. Mili, "A decentralized h-infinity unscented kalman filter for dynamic state estimation against uncertainties," *IEEE Transactions on Smart Grid*, vol. 10, no. 5, pp. 4870–4880, 2018.
[21] B. L. Nguyen, T. V. Vu, J. M. Guerrero, M. Steurer, K. Schoder, and T. Ngo, "Distributed dynamic state-input estimation for power networks of microgrids and active distribution systems with unknown inputs," *Electric Power Systems Research*, vol. 201, p. 107510, 2021.
[22] A. F. Taha, J. Qi, J. Wang, and J. H. Panchal, "Risk mitigation for dynamic state estimation against cyber attacks and unknown inputs," *IEEE Transactions on Smart Grid*, vol. 9, no. 2, pp. 886–899, 2016.
[23] G. Anagnostou and B. C. Pal, "Derivative-free kalman filtering based approaches to dynamic state estimation for power systems with unknown inputs," *IEEE Transactions on Power Systems*, vol. 33, no. 1, pp. 116–130, 2017.
[24] A. K. Singh and B. C. Pal, "Decentralized dynamic state estimation in power systems using unscented transformation," *IEEE Transactions on Power Systems*, vol. 29, no. 2, pp. 794–804, 2013.
[25] A. Gelb *et al.*, *Applied optimal estimation*. MIT press, 1974.
[26] Y. Lin and A. Abur, "A highly efficient bad data identification approach for very large scale power systems," *IEEE Transactions on Power Systems*, vol. 33, no. 6, pp. 5979–5989, 2018.
[27] T. Chen, H. Ren, P. Li, and G. A. J. Amaratunga, "A robust dynamic state estimation method for power systems using exponential absolute value-based estimator," *IEEE Transactions on Instrumentation and Measurement*, vol. 71, pp. 1–10, 2022.
[28] S. Song, P. Wu, Y. Lin, and Y. Chen, "A general dynamic state estimation framework for monitoring and control of permanent magnetic synchronous generators-based wind turbines," *IEEE Access*, vol. 9, pp. 72 228–72 238, 2021.
[29] S. Song, W. Zhang, Y. Lin, and C. Wang, "Thermo-electrical state and demand response potential estimation for power systems with building thermostats," *International Journal of Electrical Power & Energy Systems*, vol. 145, p. 108588, 2023.
[30] L. Ling, D. Sun, X. Yu, and R. Huang, "State of charge estimation of lithium-ion batteries based on the probabilistic fusion of two kinds of cubature kalman filters," *Journal of Energy Storage*, vol. 43, p. 103070, 2021.
[31] J. Qi, K. Sun, and W. Kang, "Optimal pmu placement for power system dynamic state estimation by using empirical observability gramian," *IEEE Transactions on power Systems*, vol. 30, no. 4, pp. 2041–2054, 2014.
[32] "Ieee standard for synchrophasor measurements for power systems," *IEEE Std C37.118.1-2011 (Revision of IEEE Std C37.118-2005)*, pp. 1–61, 2011.